Materials Today Bio 17 (2022) 100480

Contents lists available at ScienceDirect

Materials Today Bio

journal homepage: www.journals.elsevier.com/materials-today-bio

Positively charged nanocomplex modulates dendritic cell differentiation to enhance Th1 immune response

Yan-Wei Wu, Wan-Yu Wang, Yu-Hung Chen *

School of Medicine, College of Medicine, National Cheng Kung University, No. 1, University Road, Tainan City, 701, Taiwan, ROC

ARTICLE INFO

Keywords:
Nanocomplex
Surface charge
Dendritic cell
Cell differentiation
Th1 response

ABSTRACT

Most existing vaccines use activators that polarize the immune response to T-helper (Th) 2 response for antibody production. Our positively charged chitosan (Cs)-based nanocomplex (CNC) drives the Th1 response through unknown mechanisms. As receptors for the positively charged CNC are not determined, the physico-chemical properties are hypothesized to correlate with its immunomodulatory effects. To clarify the effects of surface charge and size on the immune response, smaller CNC and negatively charged CNC encapsulating ovalbumin are tested on dendritic cell (DC) 2.4 cells. The negatively charged CNC loses activity, but the smaller CNC does not. To further evaluate the material effects, we replace Cs by poly-amino acids. Compared with the negatively charged nanocomplex, the positively charged one preserves its activity. Using immature bone marrow-derived DCs (BMDC) enriched from BALB/c mice as a model to analyze DC differentiation, treatments with positively charged nanocomplexes evidently increase the proportions of Langerin^{+} dermal DC, CD11b^{lo} interstitial DC, and CD8a^{+} conventional DC. Additionally, vaccination with two doses containing positively charged nanocomplexes are safe and increase ovalbumin-specific IgG and recall T-cell responses in mice. Overall, a positive charge seems to contribute to the immunological effect of nanocomplexes on elevating the Th1 response by modulating DC differentiation.

1. Introduction

Biocompatible and biodegradable polymers are wildly used in medicine for applications such as dressings, sutures, stabilizers, implants, and drug delivery systems. In particular, at the nanoscale, most drug delivery systems focus on chemotherapy, gene engineering and vaccines [1–3]. In addition, various strategies can be used to form nanocomplexes, including ionic gelation, emulsion, and micellar systems. The formation strategy is selected according to the physico-chemical properties of the used materials. For charged polymers, like chitosan (Cs), ionic gelation is simpler than other strategies [4]. Cs is a positively charged polymer that allows to regulate immune responses [5]. However, as Cs has diverse chemical modifications, its key factor regulating immune responses remains unknown. We previously developed a positively charged nanocomplex (+NC) composed of two charged polymers, unmodified Cs, and non-immunogenic poly-gamma-glutamic acid (PE) to clarify the immune responses in mice. Cs derives from chitin, which is abundant in the exoskeleton of animals or in the cell walls of microorganisms. To avoid pyrogenic contamination, we use Cs with the quality of Chitoceuticals® Standard (HMC^{+}) and testing negative by Pyrochrome® Kit (Cape Cod). As a vaccine, the positively charged Cs-based nanocomplex (+CNC) can induce neutralizing antibodies and more balanced T-helper (Th) 1 and 2 responses than alum, a traditional adjuvant [6]. We found that a balanced Th response is promoted by an elevated Th1 response through unknown mechanisms. In general, naïve T cells are activated by antigen presenting cells (APCs), especially dendritic cells (DCs). Although macrophages can be activated by Cs through phagocytosis [7], the mechanisms for Cs to promote a Th1-biased immune response through DCs remain unknown. Although Cs has been observed to activate DCs through toll-like receptor 4 [8], contaminated lipopolysaccharide (LPS) renders this finding uncertain [9]. In addition to the materials, many studies have shown that the size and surface properties of a nanocomplex (NC) affect its biocompatibility rather than its immunological mechanisms [10]. In general, size influences the internalization pathway of NCs, and +NC is more likely to induce inflammatory cytokines [11]. However, the detailed mechanisms of physico-chemical properties affecting immunity have been poorly studied.

In DC activation, three important molecules on the surface mediate T-cell activation: major histocompatibility complex (MHC), costimulatory molecules, and cytokines [12]. The MHC molecules within epitopes can bind to T-cell receptors (signal 1) with the help of costimulatory

* Corresponding author.
E-mail addresses: bastawu@gmail.com (Y.-W. Wu), doriswang0817@gmail.com (W.-Y. Wang), second@mail.ncku.edu.tw (Y.-H. Chen).

https://doi.org/10.1016/j.mtbio.2022.100480
Received 16 September 2022; Received in revised form 27 October 2022; Accepted 29 October 2022
Available online 31 October 2022

Abbreviations

T helper (Th)
chitosan (Cs)
positively/negatively charged chitosan-encapsulating nanocomplex (+/−CNC)
small positively charged chitosan-encapsulating nanocomplex (+sCNC)
ovalbumin (OVA)
positively/negatively charged nanocomplex (+/−NC)
antigen presenting cell (APC)
lipopolysaccharide (LPS)
bone marrow-derived dendritic cell (BMDC)
dendritic cell (DC)
major histocompatibility complex (MHC)
positively charged poly-lysine(PK)-encapsulating nanocomplex (+PKNC)
positively charged poly-arginine (PR)-encapsulating nanocomplex (+PRNC)
negatively charged poly-glutamic acid (PE)-encapsulating nanocomplex (–PENC)
negatively charged poly-aspartic acid (PD)-encapsulating nanocomplex (–PDNC)
dynamic light scattering (DLS)
conventional dendritic cell (cDC)
tumor necrosis factor (TNF)
granulocyte-macrophage colony-stimulating factor (GM-CSF)
bone marrow-derived cell (BMC)
inflammatory dendritic cell (iDC)
migratory dendritic cell (mDC)
lymphoid resident dendritic cell (rDC)

molecules (signal 2), and then naïve T cells are activated. Simultaneously, DCs secrete cytokines (signal 3) that polarize naïve T-cell differentiation into Th1, Th2, Th17, or regulatory-T cells [13]. Considering the crucial role of DCs on T-cell activation, the +CNC can drive the Th1 response by modulating DCs.

To understand the immunomodulatory effects of size and surface properties on DCs, we designed NCs with different sizes and surface charges by various polymers encapsulating ovalbumin (OVA), which has a low endotoxin grade (Worthington Biochemical). Only +CNC induced DC 2.4 activation. Small +CNC (+sCNC) and polymers with different molecular weights formed +NCs but did not change the effect on DC 2.4 activation. In addition to +CNC, other poly-amino acids were used to form NCs with opposite surface charges by different ratios. Only +NCs activated DC 2.4 cells and showed specific patterns of differential markers. Using bone marrow-derived cells (BMCs) as a model, +NC induced $CD8a^+$ conventional DC (cDC) and $Langerin^+$ dermal DC-dominant DC population. Those DCs have been reported to be essential for generating a Th1 response. Mice inoculated with +NC showed elevated antigen-specific antibodies and CD4/8 positive T-cell activation. We found that +NCs contribute to DC differentiation and then enhance the Th1 response. Hence, the immunomodulatory effect of NCs may be adjusted by the surface charge.

2. Materials and methods

2.1. Materials

We used Cs (#24601, HMC^+, Germany); PK, PR, PE, and PD (#PLKC250, #PLR200, #PLE200, #PLD200, Alamanda Polymers, USA); Saccharides including sorbitol (#13273, Thermo Fisher Scientific, USA), glucose (#G7021, Merck, Germany), alginic acid (#A0733, TCI, Japan), mannose (#M6020, Merck, Germany), or mannans (#M7504, Merck, Germany); OVA (LS003059, Worthington Biochemical, USA); Alexa Fluor™ 660 Protein Labeling kit (#A20171, Thermo Fisher Scientific, USA); LPS (#L4391, Merck, Germany); and GM-CSF (#315–03, PeproTech, USA); DMSO (#D8418, Merck, Germany); HCl (#1943–0150, Showa, Japan); NaOH (#0812–0150, Showa, Japan).

2.2. Cell lines

DC 2.4 and RAW 264.7 cells were cultured in RPMI 1640 medium supplemented with 10% fetal bovine serum and 0.05 mM beta-mercaptoethanol. The cells were maintained at 37 °C in a humidified atmosphere containing 5% CO_2.

2.3. Encapsulation of OVA

Cs, PK or PR solution (w/v = 2.5% in 1% acetic acid or double-distilled water) was added to a PE or PD acid solution (w/v = 1% in double-distilled water) pre-mixed with 0.25 mg OVA to form positively charged nanocomplexes (+CNC, +sCNC, +PKNC, or +PRNC). The negatively charged nanocomplexes (–CNC, –PENC, or –PDNC) was formulated by increasing the ratio of PE or PD. For an uptake test, the OVA was labeled by Alexa Fluor™ 660 Protein Labeling kit following a standard protocol. All NCs contained OVA in equal volume (0.1 mg mL^{-1}) and were stored at 4 °C overnight for testing. The size, zeta potential, and polydispersity index were determined by Malvern Zetasizer Nano Series (Zetasizer Nano ZS, Malvern Panalytical, UK). The encapsulation efficiency was determined by the amount of free OVA in filtrate passing through a column with a pore size of 100 kDa.

2.4. Transmission electron microscope

A drop of NCs (1 mg mL^{-1}) was placed onto a formvar grid held by tweezers. Further, the grid was air-dried for 8 h. The samples were observed by TEM (H-7500, Hitachi, Japan) at 120 kV.

2.5. Preparation of endocytic inhibitors

The inhibitors were respectively dissolved in a proper solvent at a working concentration as following: Amiloride (#A7410, Merck, Germany), 300 mM in sterile filtered water; methyl-β-cyclodextrin (MBCD) (#C4555, Merck, Germany), 20 mM in sterile filtered water; Tannic acid (#16201, Honeywell, USA), 0.02% in sterile filtered saline; sucrose (#1.07651, Merck, Germany), 5% in sterile filtered saline; phenyl arsine oxide (PAO) (#P3075, Merck, Germany), 5 mM in DMSO; azithromycin (#75199, Merck, Germany), 132 mM in DMSO; PD-98059 (#19–143, Merck, Germany), 20 mM in DMSO; rottlerin (#557370, Merck, Germany), 40 mM in DMSO; staurosporine (#19-123-M, Merck, Germany), 300 nM in DMSO; phorbol-12-myristate-13-acetate (PMA) (#79346, Merck, Germany), 100 nM in DMSO; wortmannin (#W1628, Merck, Germany), 100 nM in DMSO.

2.6. Isolation and enrichment of immature BMDCs

We selected 6-week-old male BALB/c mice to cut the muscle and expose the femur bone above and below the joints. The center of the femur was grasped and cut above and below the joints to leave the epiphysis. The femur was transferred to a dish with 70% ethanol and then to 10% fetal bovine serum in RPMI on ice. Using a sterile tweezer to cut

each end of the bone, bone marrow was washed using a sterile syringe (28G needle). BMCs were centrifuged at 400×*g*, and sterile filtered water was added to lyse red blood cells. After 10 s, 10 × Dulbecco's phosphate buffered saline was added to stop lysis. After counting, cells were plated at a density of 1×10^6 per milliliter and maintained in RPMI medium supplemented with 10% fetal bovine serum, 0.05 mM beta-mercaptoethanol, and 25 ng mL^{-1} GM-CSF. After supplementing fresh media at days 3 and 6, immature BMDCs were harvested at day 9 for further experiments.

2.7. Ex vivo treatments with materials or charged NCs in cells

For an activation test, cell lines or BMDCs were counted and plated at a density of 2×10^5 per milliliter in a 12-well plate. Different groups of cells were treated by appointed amounts of materials as follows. For cell lines, we added 1.25 μg of LPS, 20 μL of +CNC or +sCNC and 5, 10, 20, 40, or 80 μL of –CNC as well as 10, 5, 2.5, or 1.25 μL of +PKNC, +PRNC, –PENC, or –PDNC in the culture medium. For BMDCs, we added 1 μg of OVA only, 1 μg of OVA mixing 1.25 μg of LPS, 10 μL of +sCNC and 10, 5, or 2.5 μL of +PKNC, +PRNC, –PENC, or –PDNC in the culture medium. After 24-h incubation, cells were harvested for typing surface markers. For an uptake test, cell lines were counted and plated at a density of 2×10^5 per milliliter in a 12-well plate. Cells were pre-incubated with inhibitors for 1 h, and 1 μg of OVA-Alexa 660 or 20 μL of +CNC encapsulating 1 μg of OVA-Alexa 660 were added in the culture medium. After 4-h incubation, cells were harvested for the detection of fluorescence.

2.8. Surface staining of cells

Upon treatments with materials or charged NCs for the appointed time, cells were collected and kept at 4 °C for 40-min surface staining with appointed antibodies including MHC-I-FITC (#MA5-17999), MHC-II-FITC (#562003), MHC-II-SPRD (#1895–13), MHC-II-PE (#1895–09), CD11b-BV510 (#562950), CD11c-APC (#561119), CD8-APC-H7 (#560182), Langerin-PE-Vio770 (#130-107-150), CD107b-PerCP-Cy5.5 (#564248), DCIR-2-BB515 (#565171), and CD209a-BV421 (#747827). The corresponding isotype antibodies were mouse IgG-FITC (#11-4724-81), mouse IgG2a-FITC (#555573), rat IgG2b-PE (#0118–09), rat IgG2b-BV510 (#562951), hamster IgG1-APC (#553956), rat IgG2a-APC-H7 (#560197), rat IgG2a-PE-Vio770 (#130-102-647), rat IgG2a-PerCP-Cy5.5 (#560722), rat IgG2b-BB515 (#564421), and rat IgG2a-BV421 (#562602). The antibodies were purchased from BD Biosciences (USA), SouthernBiotech (USA), or Miltenyi Biotec (Germany). After washing twice with phosphate-buffered saline, cells were fixed with 2% paraformaldehyde for FACSLyric analysis (BD Biosciences).

2.9. Mice vaccination

Six-week-old male BALB/c mice were injected two doses of materials through a subcutaneous route beginning at day 0 in a 14-day interval. The volume per dose was 100 μL. All materials contained OVA in equal volume (0.1 mg mL^{-1}). Sera were sampled from the facial vein at days 0, 14, 21, and 28. Mice were sacrificed at day 28 to evaluate spleen enlargement and recall response.

2.10. Enzyme-linked immunosorbent assay

Standard IgG or OVA was coated on 96-well plates at appropriate concentrations overnight at 4 °C. Mouse sera were serially diluted and added into the wells for 2 h at room temperature (18–27 °C). *Anti*-IgG antibodies conjugated to horseradish peroxidase were added into the wells for 1 h at room temperature. Then, TMB substrate was added to the sample for color development, and the reaction was stopped using 2 N HCl. Finally, the absorbance per well was measured using a microplate reader (Infinite M200 Pro, Tecan Trading, Switzerland) at a wavelength of 450 nm.

2.11. Recall response of T cells

At day 28 after the first injection, 2×10^5 splenocytes were placed in a 24-well plate and incubated with 2 μg OVA per well for 5 days. Splenocytes were collected and kept at 4 °C for 40-min surface staining with appointed antibodies including CD3 (#553062), CD25 (#551071), CD4 (#553051), and CD8 (#553032) to then analyze flow cytometry. Antibodies were purchased from BD Biosciences (USA).

2.12. Statistical analyses

Values were presented as mean ± standard deviation and obtained from one-way analysis of variance (ANOVA). We used notation *,# for $p < 0.05$, **,## for $p < 0.01$, and ***,### for $p < 0.001$. We used $n = 3$ per cell line group and $n = 3$ for the mock mouse group, $n = 4$ for the OVA only group, and $n = 5$ for the OVA + LPS, +sCNC, +PKNC, +PRNC, –PENC, and –PDNC groups.

2.13. Study approval

Animal experiments were conducted in accordance with the "Guideline for the Care and Use of Laboratory Animals" as defined by the Council of Agriculture, Taiwan and were approved by the Laboratory Animal Center, College of Medicine, National Cheng Kung University (IACUC number: 108036 and 109079).

3. Results

3.1. Activity of positively charged Cs or poly-amino acids encapsulating NCs on DC 2.4 cells

We first encapsulated OVA by Cs and PE to form +CNC (409.7 nm, 37.2 mV) as in our previous study (Fig. 1A and B). Various studies have reported the immunologic activity of Cs in vaccines [14–16], but the mechanisms and receptors involved are still unclear [17]. To evaluate physico-chemical effects of +CNC on immune responses, we changed the ratio of Cs and PE to form the –CNC (372.2 nm, −53.7 mV) (Fig. 1C and D). The images of the +CNC and –CNC were observed by transmission electron microscope which were comparable with DLS results (Fig. 1E). Besides, both CNCs were nearly monodisperse and with a high encapsulation efficiency of antigen (Fig. 1F). After applying the +CNC to DC 2.4 cells for 24 h, surface expression of MHC-I and -II, which represent antigen presentation and activation of DCs [18], was induced, differing from the –CNC application with increased doses (Fig. 1G and H). Hence, the positive zeta potential of nanomaterials is more likely to be internalized into cells [19]. Moreover, when the pH value of +CNC was adjusted to 4 by HCl, the zeta potential was obviously increased. Along with increased pH adjusted by NaOH, the zeta potential was decreased until the pH was equal to 6, which made +CNC swelling and inhomogeneous (Fig. 1I). The activation of DC 2.4 induced by +CNC was obviously enhanced by the increase of zeta potential (Fig. 1J and K). Accordingly, the property and degree of zeta potential on +CNC were highly related to the DC 2.4 activation. However, the zetapotential of nanomaterials is not conclusively related to DC activation due to a lack of detailed study [20].

3.2. Saccharide and size effects of positively charged Cs or poly-amino acids encapsulating NCs on DC 2.4 cells

To further determine the charge effect of +CNC on DC activation, the characteristics of saccharide and size were manipulated. First, Cs in the +CNC was replaced by positively charged poly-amino acids, including poly-lysine (PK) and poly-arginine (PR). The negatively charged polymers included PE and poly-aspartic acid (PD). These simple peptides are

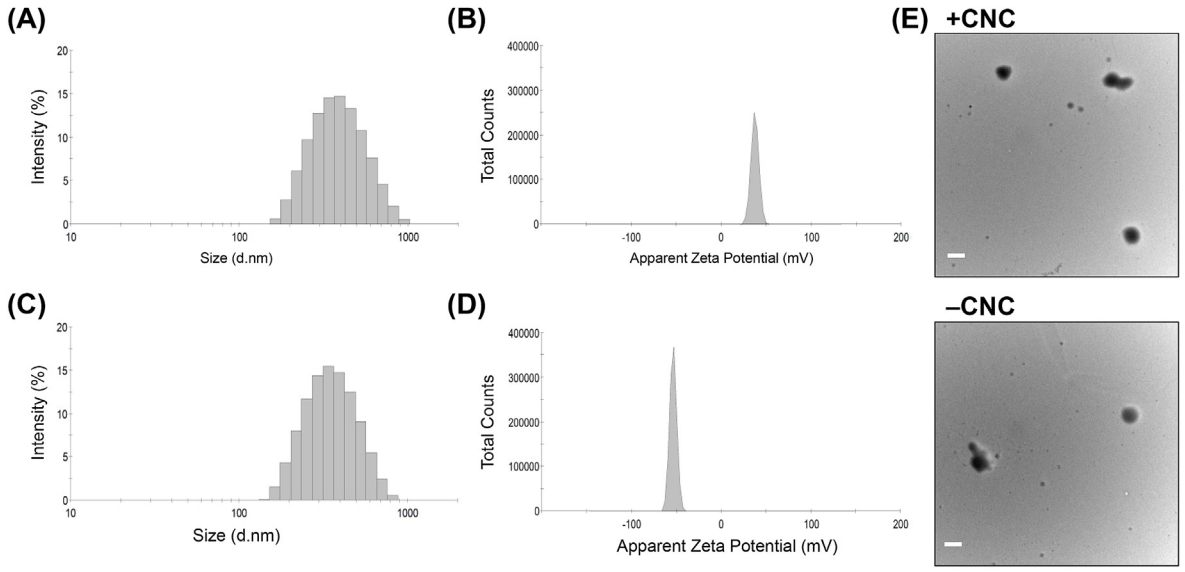

(F)

NCs	Z-average (d. nm)	Polydispersity index	Zeta potential (mV)	Encapsulation efficiency (%)
+CNC	409.7	0.138	37.2 ± 4.34	> 98.5
–CNC	372.2	0.123	-53.7 ± 3.87	> 98.5

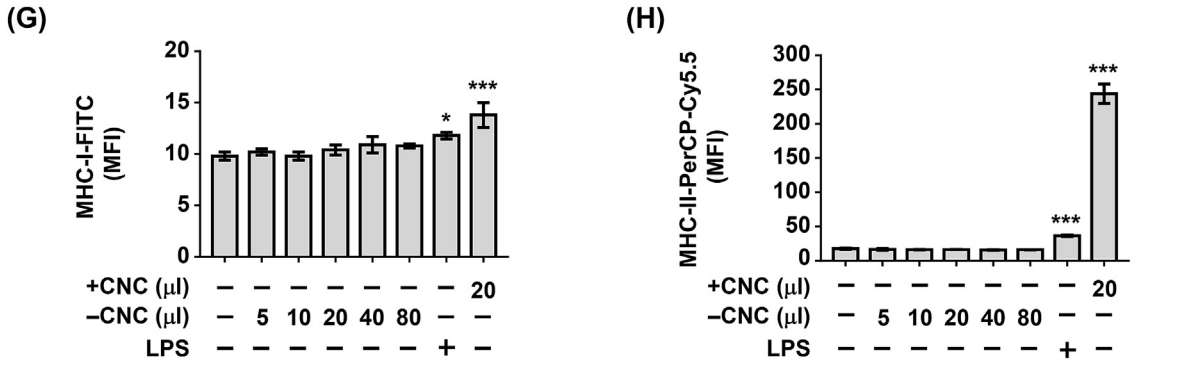

(I)

pH	Z-average (d. nm)	Polydispersity index	Zeta potential (mV)
+CNC (5-6)	454.7	0.152	40.5 ± 4.61
4	458.7	0.178	61.1 ± 4.05
5	415.5	0.185	56.7 ± 3.81
6	667.3	0.784	31.4 ± 3.80

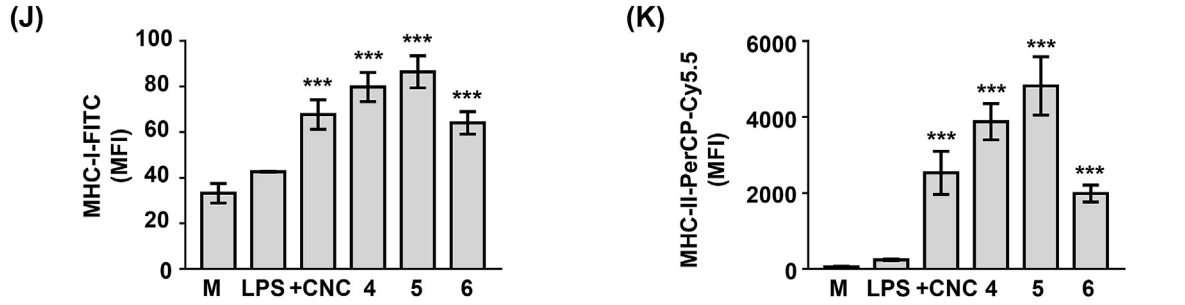

(caption on next page)

Fig. 1. The physical characteristics of +CNC or –CNC and its opposite activities on DC 2.4 cells. (A–D) Diameters and zeta potentials of +CNC (A,B) and –CNC encapsulating OVA (C,D), with final OVA concentration of 0.1 mg mL^{-1} detected by DLS. (E) The images of +CNC or –CNC by transmission electron microscope. Scale bar: 500 nm. (F) Polydispersity index and encapsulation efficiency of +CNC and –CNC determined from DLS or fluorescence intensity from free OVA. (G,H) After 24-h incubation with LPS, +CNC, or –CNC, the surface MHC-I (G) and -II (H) were analyzed by specific antibodies conjugating fluorescence for detection of flow cytometry. (I) Diameter, zeta potential, and polydispersity index of +CNCs within different pH values ranged from 4 to 6 and determined from DLS. (J,K) After 24-h incubation with +CNCs within different pH values, the surface MHC-I (J) and -II (K) were analyzed by specific antibodies conjugating fluorescence for detection of flow cytometry. Values are presented as mean ± standard deviation, $n = 3$. Statistical analyses were performed by one-way ANOVA followed by Tukey's multiple comparisons test. *, compared with untreated group. *$p < 0.05$, ***$p < 0.001$.

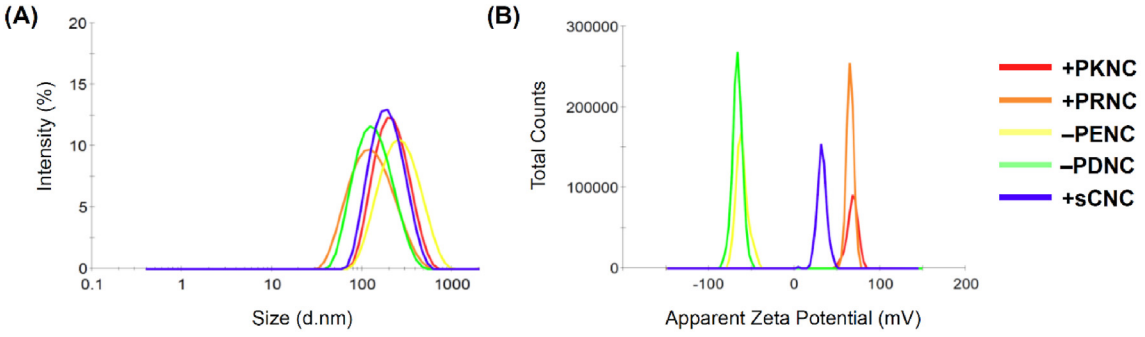

(C)

NCs	Z-average (d. nm)	Polydispersity index	Zeta potential (mV)	Encapsulation efficiency (%)
+PKNC	190.8	0.293	66.2 ± 6.71	> 98.5
+PRNC	116.8	0.253	64.7 ± 4.18	> 98.5
–PENC	226.5	0.243	-61.1 ± 6.92	> 98.5
–PDNC	123.3	0.212	-66.5 ± 5.96	> 98.5
+sCNC	172.2	0.142	31.8 ± 5.67	> 98.5

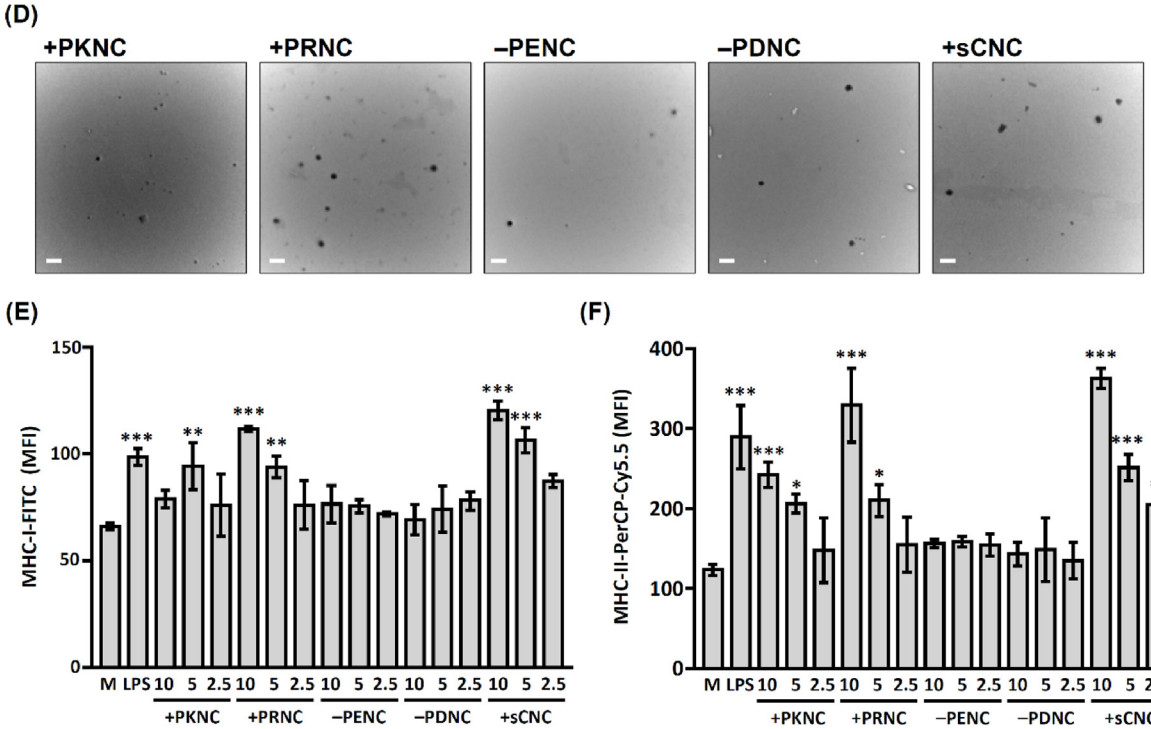

Fig. 2. Physical characteristics of poly-amino-acid-based NCs with completely opposite surface charge and activities on DC 2.4 cells. (A,B) Diameters (A) and zeta potentials (B) of OVA encapsulating +PKNC, +PRNC, –PENC, –PDNC, and +sCNC with final OVA concentration of 0.1 mg mL^{-1} detected by DLS. (C) Polydispersity index and encapsulation efficiency of +PKNC, +PRNC, –PENC, –PDNC, and +sCNC determined from DLS or fluorescence intensity from free OVA. (D) The images of +PKNC, +PRNC, –PENC, –PDNC, and +sCNC by transmission electron microscope. Scale bar: 500 nm. (E,F) After 24-h incubation with 1.25 μg of LPS, 10 μL of +PKNC, +PRNC, –PENC, –PDNC or +sCNC, the surface MHC-I (E) and -II (F) were analyzed by specific antibodies conjugating fluorescence for detection of flow cytometry. Values are presented as mean ± standard deviation, $n = 3$. Statistical analyses were performed by one-way ANOVA, followed by Tukey's multiple comparisons test. *, compared with untreated group (mock). *$p < 0.05$, **$p < 0.01$, ***$p < 0.001$.

known to be poorly immunogenetic in the immune system [21]. By manipulating the polymer ratios, two groups of oppositely charged NCs encapsulating equal OVA amounts were prepared (PK and PE form +PKNC or –PENC; PR and PD form +PRNC or –PDNC). The diameters and zeta potentials of four NCs were determined by dynamic light scattering (DLS) (Fig. 2A and B) ranging from 123.3 to 226 nm and −66.5 to 66.2 mV. In addition, +sCNC was prepared (172.2 nm, 31.8 mV) as a control. The five NCs were controlled within nearly same size and monodisperse and showed a high encapsulation efficiency of antigen (Fig. 2C). The electron microscopic images of the five NCs were consistent with DLS results (Fig. 2D). Compared with +sCNC, +PKNC and +PRNC equivalently induced MHC-I and -II expressions but –PENC and –PDNC did not (Fig. 2E and F).

To evaluate the effect of saccharide on +CNC-induced DC activation, several saccharides were added in +PKNC to form +NCs with nearly same size and monodisperse as +sCNC (Fig. 3A). Compared with +PKNC without saccharide, the +NCs with saccharide did not further induce MHC-I and -II expressions of DC 2.4 cells (Fig. 3B and C), which showed an invalid role of saccharide on DC activation. In addition, changing the molecular weight of the poly-amino acids did not affect DC activation (Fig. S1). Hence, the positive charge of NCs seems to play a crucial role in DC activation. The materials of NCs, size and molecular weight are not restricted to be saccharide or within a specific range.

3.3. The endocytic mechanisms for +CNCs on DC 2.4 cells

Because of the opposite charge between +CNC and plasma membrane, +CNC was easily absorbed to the membrane for further uptake. The APCs engulf foreign materials through various endocytic mechanisms for antigen presentation. To understand the intracellular mechanism of +CNC, endocytic mechanisms for its uptake needs to be defined first. We conjugated OVA with Alexa 660 fluorescence for the intracellular detection, and added different inhibitors for endocytic mechanisms to clarify the pathway involved (Fig. 4A). In case of free OVA uptake, broad inhibitors like tannic acid or ice certainly inhibited its uptake. Further, fluid phase endocytosis and macropinocytosis were known to be utilized by free OVA which was consistent with our results (Fig. 4B). Few inhibitors were observed to increase the uptake of free OVA that might be caused by complementary effects. On the other hand, compared with free OVA, +CNC uptake was closely related to caveolin, ipid raft, clathrin or unknown receptors (Fig. 4C). Accordingly, the endocytic pathways induced by +CNC seem to be very different from free OVA.

3.4. Cytokine production and surface markers induced by +NCs on DC 2.4 cells

To understand the NC charge effect on DC, activation/differentiation markers [22] and cytokines were analyzed in DC 2.4 cells. In general, CD11b is a pan-myeloid marker [23], and CD11c is expressed on DCs in a highly activation-dependent manner, like MHC-II. For the DC subtype expressing CD8a, it can uniquely prime $CD8^+$ T cells. In mouse subsets of DC ($CD11c^+$), plasmacytoid DCs were characterized with positive MHC-II [24]. In addition, the cDC with positive MHC-II can be further divided into cDC1 with positive CD8a and cDC2 with positive CD11b [25]. After treating materials including +sCNC and +PKNC, CD11b, CD8a, MHC-II and CD11c were generally elevated (Fig. 4D–G). In addition to surface markers, cytokines secreted from DC 2.4 and RAW 264.7 cells upon treatment with +sCNC or +PKNC were detected (Fig. S2). +PKNC induced interleukin-4 production (Fig. S2B), and +sCNC induced tumor necrosis factor (TNF)-α production (Fig. S2E). On the other hand, –CNC did not induce cytokine productions on APCs.

Compared with LPS, although +NCs did not strongly induces cytokines, they activated APCs to express both activation and differentiation markers. As DC 2.4 cells are artificially created from bone marrow isolates of C57BL/6 mice [26], they are transduced with retrovirus vectors expressing murine granulocyte-macrophage colony-stimulating factor (GM-CSF) and with oncogenes *Myc* and *Raf* [27]. Consequently, this may not be a proper model to reflect the differential scenario of DCs in mice.

3.5. Bone marrow-derived DC differentiation modulated by +NCs

To mimic the naïve DC differentiation in mice, we isolated BMCs from murine femur and enriched an immature bone marrow-derived DC (BMDC) population supplementing with 25 ng mL^{-1} GM-CSF in a medium for 9 days [28] (Fig. 5A). Using BMDCs, DC differentiation by NCs was further evaluated. We arranged eight surface markers for typing DC subsets [29,30] (Fig. 5B-N), and the resulting typing chart is shown in Fig. S3. With a proper hierarchy gating in dotplot by isotype staining (Fig. S4), DC subsets were characterized in one vial of cells. In brief, DC subsets in mouse can be distinguished into four groups by different functions [31]: plasmacytoid DC, inflammatory DC (iDC), migratory DC (mDC) and lymphoid resident DC (rDC). Plasmacytoid DCs locate in lymphoid organs for the detection of pathogen-derived nucleic acids and respond with rapid and massive production of type-I interferon. iDCs are recruited to an inflammation site for multi-function in innate defense (NO and TNF-α production) and T-cell activation. mDCs circulate in tissues and migrate from local to lymph nodes to initiate and expand T-cell responses. rDCs remain in lymphoid organs to initiate and expand T cell responses. In our results, with a supplement of GM-CSF (mock), BMDC was enriched to over 60% in BMC, mostly obtaining iDCs (monocyte-derived DC) and mDCs (Langerin$^-$ dermal DC and $CD11b^{hi}$ interstitial DC). Treatment with LPS mixing OVA or OVA only showed similar patterns to those of the mock group. For +sCNC treatment, several mDCs (TIP-DC, $CD11b^{lo}$ interstitial DC, and Langerin$^+$ dermal DC) (Fig. 5D,M, N) and rDCs ($CD8a^+$ cDC) (Fig. 5F,H) increased in the BMDC population. Moreover, +PKNC or +PRNC treatment induced proportions of mDCs ($CD11b^{lo}$ interstitial DC and Langerin$^+$ dermal DC) (Fig. 5M and N) and rDCs ($CD8a^+$ cDC and $CD8a^-$ cDC) (Fig. 5F,H,J) in BMDCs. However, –PENC or –PDNC treatment showed no difference with the mock group.

In addition to typing individual DC subsets, we organized a pie chart to represent the proportion of individual DC subsets in the rDC and mDC groups. Clearly, treatment with three +NCs (+sCNC, +PKNC, and +PRNC) increased the proportion of $CD8a^+$ cDCs in both rDC and DC populations (Fig. 6A). For the mDC group, treatment with +NCs increased the proportions of Langerhans$^+$ dermal DC and $CD11b^{lo}$ interstitial DC (Fig. 6B). To understand the population change in four DC groups, we deducted the overlapping percentage by a Venn diagram and then calculated proportion of each DC group (Fig. S5). Treatments with GM-CSF only (mock), OVA only, LPS mixing OVA, and two –NCs (–PENC or –PDNC) drove an iDC-dominant DC population (Fig. 6C). On the other hand, three +NC treatments increased the rDC group but decreased the iDC group dominantly. In addition, we observed a dose-dependent effect of the three +NC treatments. Accordingly, the positive charge seems to play an important role in increasing rDC population and decreasing iDC population. The increase in rDC population is dominantly $CD8a^+$ cDCs. Although the mDC group showed no difference in the three +NC treatments, the population changed to Langerhans$^+$ dermal DC and $CD11b^{lo}$ interstitial DC dominantly.

3.6. Antibody production and recall T cell responses induced by +NCs in BALB/c mice

To confirm the immune response triggered by the three evaluated +NCs, they were injected to BALB/c mice subcutaneously in two doses in a 14-day interval. The safety of the three +NCs was determined by spleen enlargement assessment at day 28 post-injection (Fig. 7A). OVA-specific IgG in sera at day 28 was elevated in mice groups injected with LPS mixing OVA or three +NCs (Fig. 7B), but two –NCs showed no effects. In addition, the antigen-specific recall T-cell responses were analyzed by applying OVA to splenocytes from vaccinated mice. The $CD4^+$ T cells (Fig. 7C) from groups vaccinated by LPS mixing OVA or three +NCs were activated, and the activation was relatively elevated with OVA

(A)

Saccharide +NCs	PK:PE:Saccharide (weight ratio)	Z-average (d. nm)	Polydispersity index	Zeta potential (mV)
+PKNC	65:8:0	208.9	0.169	66.7 ± 4.33
Sorbitol +PKNC	65:8:8	189.5	0.223	65.4 ± 4.32
Glucose +PKNC	65:8:16	186.0	0.124	69.3 ± 3.74
Alginic acid +PKNC	65:8:2	229.6	0.273	62.8 ± 5.49
Mannose +PKNC	65:8:16	192.4	0.153	65.8 ± 5.86
Mannans +PKNC	65:8:12	169.4	0.292	63.5 ± 5.48
Chitosan +PKNC	65:8:12.5	163.6	0.223	43.3 ± 4.16

(B)

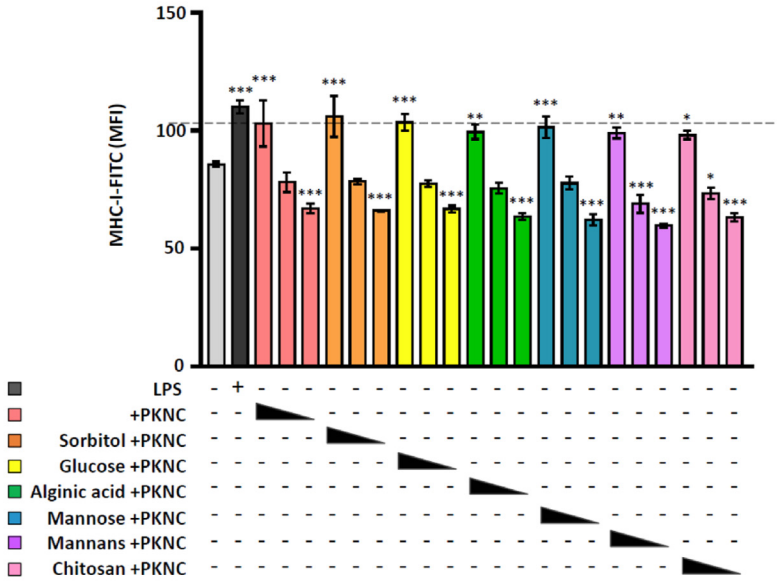

(C)

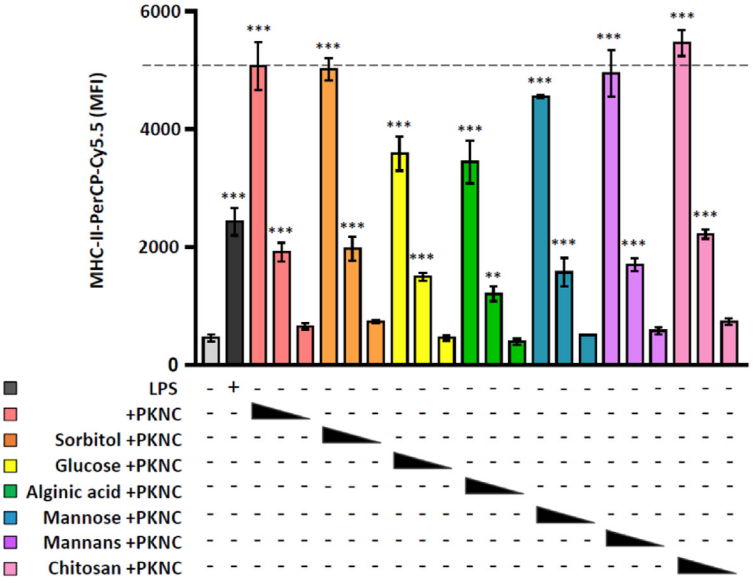

Fig. 3. Activities of various saccharides encapsulating +PKNCs on DC 2.4 cells. (A) Saccharides encapsulating +PKNCs were fabricated with different weight ratio of PK, PE, and saccharides including sorbitol, glucose, alginic acid, mannose, mannans, or chitosan. Diameters, polydispersity index, and zeta potentials were detected by DLS. (B,C) After 24-h incubation with 1.25 μg of LPS, 80, 50, or 40 μL of saccharides encapsulating +PKNCs, the surface MHC-I (B) and -II (C) were analyzed by specific antibodies conjugating fluorescence for detection of flow cytometry. Values are presented as mean ± standard deviation, $n = 3$. Statistical analyses were performed by one-way ANOVA, followed by Tukey's multiple comparisons test. *, compared with untreated group. *$p < 0.05$, **$p < 0.01$, ***$p < 0.001$.

(A)

#	inhibitors	Endocytosis pathway inhibited
1	Amiloride	Fluid Phase Endocytosis (FPE)
2	MBCD	Caveolin-dependent and lipid raft-dependent
3	Tannic acid	All endocytosis
4	Hypertonic sucrose	Clathrin-coated vesicle-mediated
5	ice	All endocytosis
6	DMSO	Solvent control
7	PAO	Receptor-mediated
8	Azithromycin	FPE
9	PD-98059	FPE
10	Rottlerin	FPE, but not receptor-mediated
11	Staurosporine	FPE (inhibits protein kinase C)
12	PMA	Activates protein kinase C (enhances FPE?)
13	Wortmannin	Macropinocytosis and Fc-mediated phagocytosis

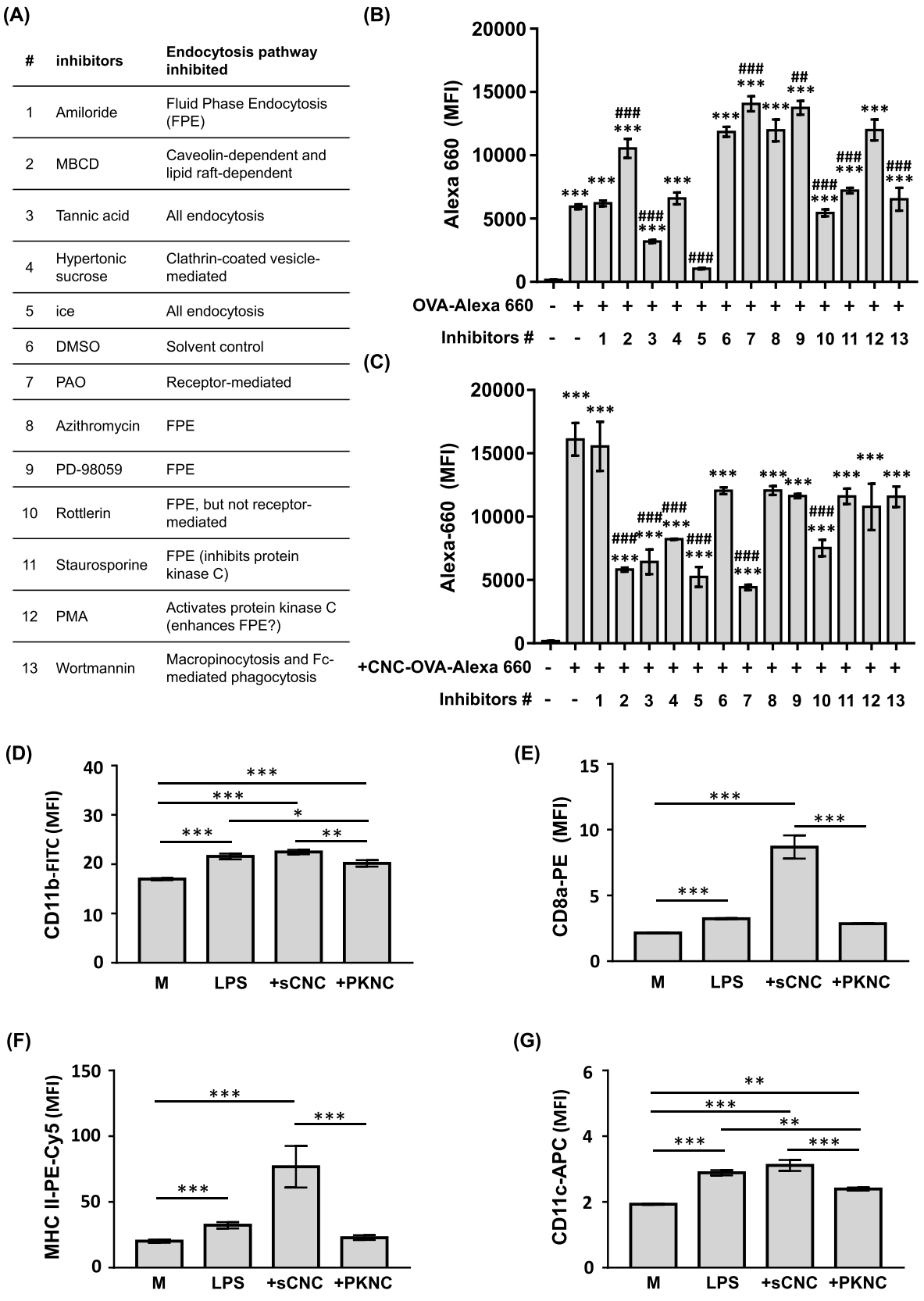

Fig. 4. Endocytic mechanisms and surface markers on APCs induced by positively charged NCs. (A) Inhibitors for various pathways of endocytic mechanism. (B,C) After incubation with endocytic inhibitors for 1 h, DC 2.4 cells were treated with OVA-Alexa 660 (B) or +CNC encapsulating OVA-Alexa 660 (C) for 4-h incubation. The fluorescence was detected by flow cytometry. (D–G) After treatment with LPS, +sCNC or +PKNC, surface markers including CD11b (D), CD8a (E), MHC-II (F), and CD11c (G) on DC 2.4 and RAW 264.7 cells were analyzed by specific antibodies conjugating fluorescence for detection of flow cytometry. Values are presented as mean ± standard deviation, $n = 3$. Statistical analyses were performed by one-way ANOVA followed by Tukey's multiple comparisons test. *, compared with untreated group (mock). #, compared with solvent only. $^{*}p < 0.05$, $^{**,\#\#}p < 0.01$, $^{***,\#\#\#}p < 0.001$.

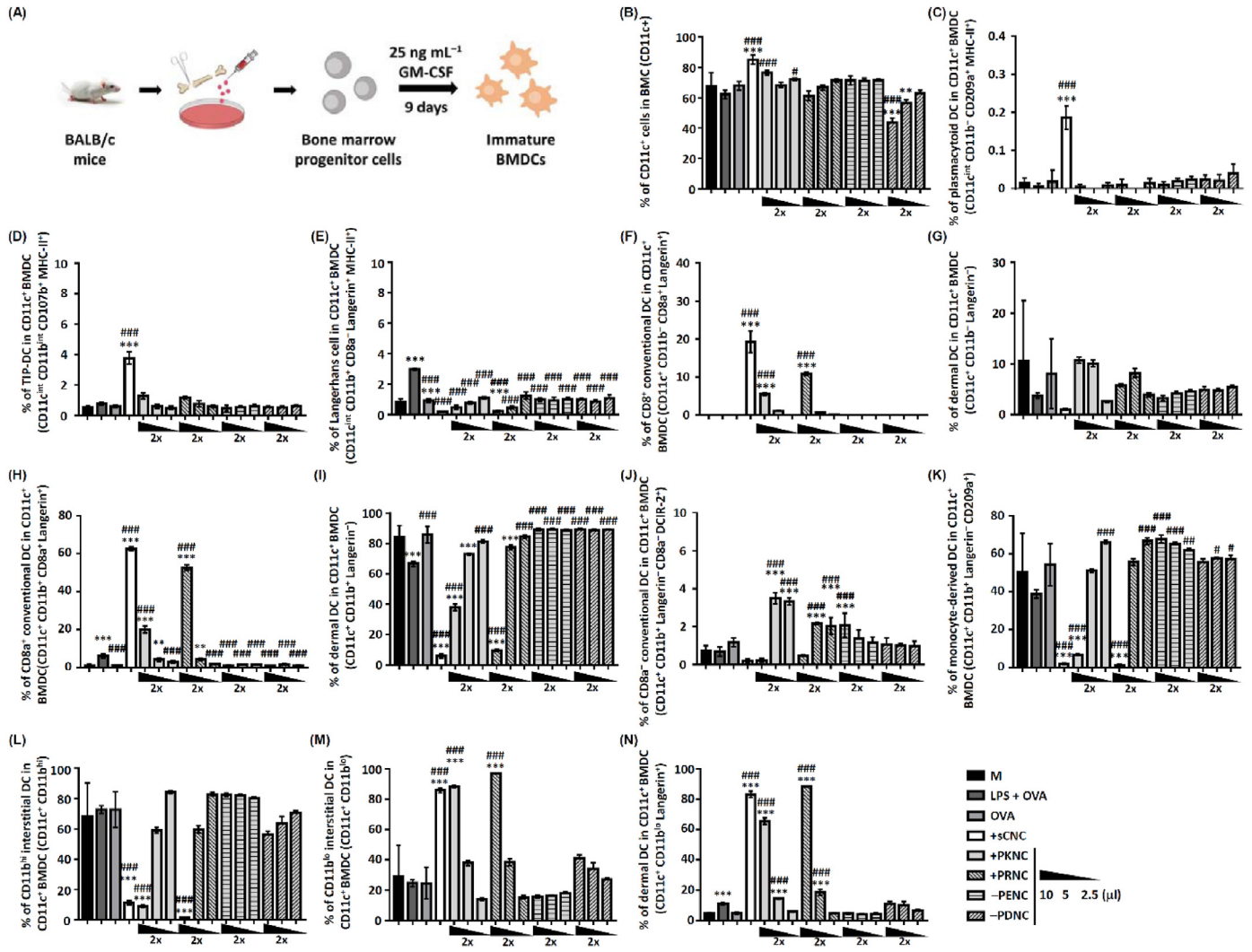

Fig. 5. Typing subsets of BMDCs in treatments with charged NCs. (A) BMCs were isolated from BALB/c mice and then enriched by 25 ng mL^{-1} GM-CSF for 9 days to become immature BMDCs. (B) Proportion of $CD11c^+$ cells (BMDCs) in total BMCs. (*C*–N) Proportions of plasmacytoid DCs (C), TIP-DCs (D), Langerhans cells (E), $CD11b^-$ $CD8a^+$ cDCs (F), $CD11b^-$ $Langerin^+$ dermal DCs (G), $CD11b^+$ $CD8a^+$ cDCs (H), $CD11b^+$ $Langerin^-$ dermal DCs (I), $CD8a^-$ cDCs (J), monocyte-derived DCs (K), $CD11b^{hi}$ interstitial DCs (L), $CD11b^{lo}$ interstitial DCs (M), and $CD11b^{lo}$ $Langerin^+$ dermal DCs (N) in BMDCs treated by appointed materials or charged NCs. Values are presented as mean ± standard deviation, $n = 3$. Statistical analyses were performed by one-way ANOVA followed by Tukey's multiple comparisons test. *, compared with untreated group (mock). #, compared with LPS mixing OVA. $^{\#}p < 0.05$, $^{**,\#\#}p < 0.01$, $^{***,\#\#\#}p < 0.001$.

coincubation for 5 days. The $CD8^+$ T cells presented a similar pattern only in groups vaccinated by the three +NCs but not in the group vaccinated by LPS mixing OVA (Fig. 7D). These results indicate that positive charges contribute to elevated Th responses, especially the Th1 response, by modulating DC differentiation.

4. Discussion

The immunomodulatory effect of NC is governed by various factors including size, composition, morphology, and surface charge. The size of NC is especially important to the pharmacokinetic. In general, smaller NC (<500 nm) circulates through the venous and lymphatic vessels to increases antigen presentation [32]. By manipulating composition and morphology, NC can be sensitive to factors such as pH, temperature, and photon to affect its pharmacokinetic. Regarding the surface charge of NC, cell targeting and clearance are evaluated mostly. However, it is rarely addressed whether surface charge is the key factor of NC to activate immune system. The reason is that various strategies including chemical modification and additives are used to fabricate NC for increasing the immunomodulatory effect. In addition, an appropriate control of oppositely charged NC is not always available because the complexity of formation strategy. In this study, we fabricated NCs with the similar size and opposite surface charges by same materials which made results comparable. Though we proved the contribution of positive charge to immune activation, it does not mean that only positively charged NC can activate immune response. The additives including diethylaminoethyl-dextran, toll-like receptor agonists, or cytokines perform immune activators even in negatively charged platforms [33–35]. Moreover, our system is performed in an artificial condition with consistent plasma proteins from bovine serum albumin. Even when our NC applied to intradermal injection, the plasma proteins are quite rare in that region which makes our finding comparable. However, the absorbed plasma proteins need to be considered when NC circulates in blood. The plasma proteins can bind to NC through electricity and topography dependent manners. Though the precise rules of protein absorbed on NC remain unknown, the corona has been proved to affect uptake, bio-distribution, and clearance [36], which indirectly influence immune activation of NC.

The signaling pathways for *N*C-induced DC differentiation remain unclear. Few studies hypothesize the toll-like receptor 4 as the chitosan's

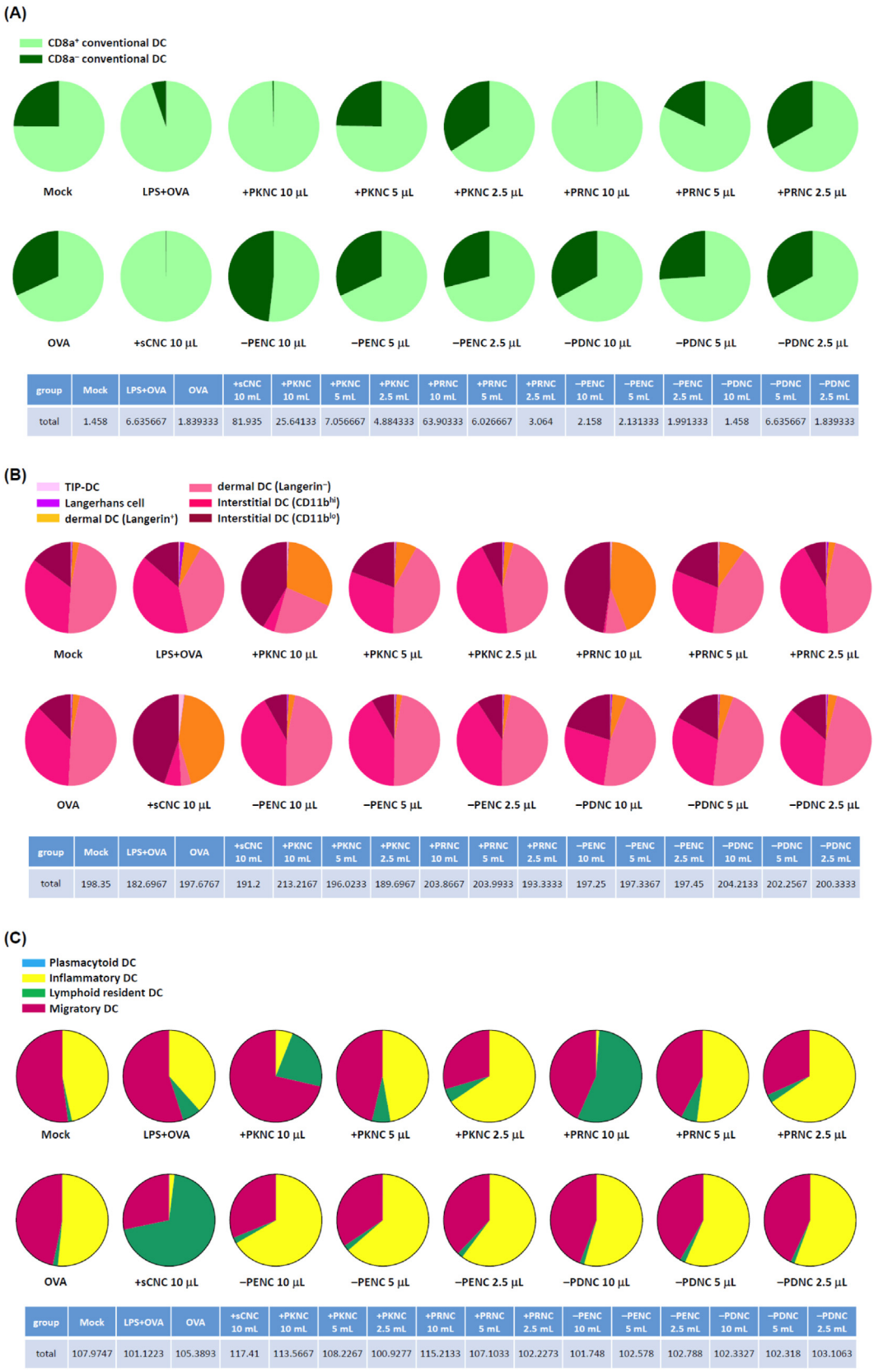

group	Mock	LPS+OVA	OVA	+sCNC 10 mL	+PKNC 10 mL	+PKNC 5 mL	+PKNC 2.5 mL	+PRNC 10 mL	+PRNC 5 mL	+PRNC 2.5 mL	−PENC 10 mL	−PENC 5 mL	−PENC 2.5 mL	−PDNC 10 mL	−PDNC 5 mL	−PDNC 2.5 mL
total	1.458	6.635667	1.839333	81.935	25.64133	7.056667	4.884333	63.90333	6.026667	3.064	2.158	2.131333	1.991333	1.458	6.635667	1.839333

group	Mock	LPS+OVA	OVA	+sCNC 10 mL	+PKNC 10 mL	+PKNC 5 mL	+PKNC 2.5 mL	+PRNC 10 mL	+PRNC 5 mL	+PRNC 2.5 mL	−PENC 10 mL	−PENC 5 mL	−PENC 2.5 mL	−PDNC 10 mL	−PDNC 5 mL	−PDNC 2.5 mL
total	198.35	182.6967	197.6767	191.2	213.2167	196.0233	189.6967	203.8667	203.9933	193.3333	197.25	197.3367	197.45	204.2133	202.2567	200.3333

group	Mock	LPS+OVA	OVA	+sCNC 10 mL	+PKNC 10 mL	+PKNC 5 mL	+PKNC 2.5 mL	+PRNC 10 mL	+PRNC 5 mL	+PRNC 2.5 mL	−PENC 10 mL	−PENC 5 mL	−PENC 2.5 mL	−PDNC 10 mL	−PDNC 5 mL	−PDNC 2.5 mL
total	107.9747	101.1223	105.3893	117.41	113.5667	108.2267	100.9277	115.2133	107.1033	102.2273	101.748	102.578	102.788	102.3327	102.318	103.1063

Fig. 6. Proportions of individual DC subsets in rDCs, mDCs and BMCs in treatments of charged NCs. (A,B) Pie charts of proportions of individual DC subsets in rDCs (A) or mDCs (B) for treatments with appointed materials or charged NCs. (C) Proportions of individual DC subsets deducted from overlapping percentage in Venn diagrams. Values are presented by proportion of each DC group in BMCs. The tables below the pie charts show the sum of individual DC subsets in each DC group. Individual DC subsets are color-coded.

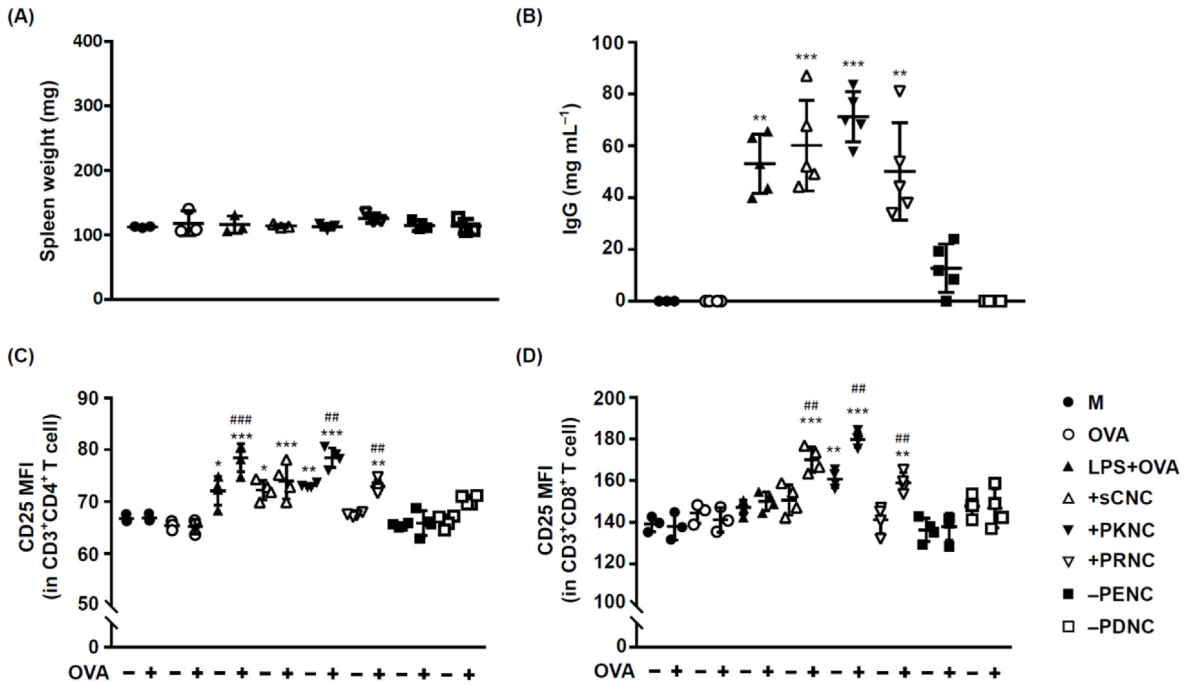

Fig. 7. Antibody and T-cell responses in BALB/c mice vaccinated by charged NCs. BALB/c mice were subcutaneously injected with two doses of appointed materials or charged NCs in a 14-day interval. (A,B) At day 28 after the first injection, spleen enlargement (A) was measured to evaluate the vaccine. Titers of OVA-specific IgG in mice sera (B) were determined by enzyme-linked immunosorbent assay. (C,D) At day 28 after the first injection, splenocytes were collected and incubated with OVA. To evaluate the antigen specific activation of T cells, the surface CD3, CD25 and CD4 (C) or CD8 (D) were stained by appointed antibodies and fixed for flow cytometry analysis. Values are presented as mean ± standard deviation, $n = 3$. Statistical analyses were performed by one-way ANOVA followed by Tukey's multiple comparisons test. *, compared with treated/untreated (mock) group. #, compared with individual untreated group. $^{*}p < 0.05$, $^{**,\#\#}p < 0.01$, $^{***,\#\#\#}p < 0.001$.

receptor to activate DC. In our finding, poly-amino-acids could induce DC activation, and LPS induced DC differentiating to a distinct population compared with +NCs. It addresses that +NCs activate DC through a distinct signaling pathway from LPS. After activation and differentiation, DCs secret cytokines and express different surface markers [37]. In general, the GM-CSF induced BMDCs is majorly defined as the progenitor of cDCs [38]. However, it was recently descripted that GM-CSF induced BMDCs in fact yield a combination of monocyte-derived cells and cDC-like cells [39]. Because the undefined cell types of GM-CSF induced BMDCs, it is hard to type it by only few surface markers. Therefore, we chose at least three positive or negative markers for each type of DCs. In our typing assay of BMDCs, the treatments of +NC seemed to be ineffective to change the proportion of plasmacytoid DCs (Fig. 5C). The reason could be that mouse plasmacytoid DCs were recently found to predominantly originate from a progenitor distinct from that of most cDCs [40]. Therefore, the effects on plasmacytoid DCs need to be further evaluated by other suitable models. Regarding the proportion of mDCs, three +NCs increase Langerin^{+} dermal DCs, indicating high mobility cross-presenting antigen to CD8^{+} T cells, and promoting the development of cytotoxic T-lymphocyte responses. Accordingly, the three evaluated +NCs can induce CD8^{+} T-cell activation in mice. Interestingly, there is a subtle difference between Cs- and poly-amino-acid-based NCs in TIP-DCs and CD8a^{-} cDCs. TIP-DCs produce TNF/inducible NO synthase for bacteria defense and CD8^{+} T-cell proliferation and increase TIP-DCs in the +CNC group co-responding to more TNF-α secretion in DC 2.4 and RAW 264.7 cells (Fig. S2E). In addition, CD8a^{-} cDCs present antigen to naïve CD4^{+} T cells in an MHC-II context inducing either helper or regulatory T cells. Increasing CD8a^{-} cDCs in the poly-amino-acid-based NC group co-responds to more interleukin-4 secretion in DC 2.4 and RAW 264.7 cells (Fig. S2B). It seems that the +CNC has a stronger effect on CD8^{+} T cells, while the poly-amino-acid-based NC is better on CD4^{+} T cells. Actually, foreign antigens always pass several intracellular organelles and vesicles that determine their final destiny. For example, antigens getting into endosome and then fusing with lysosome will be degraded by proteinases. Without escaping from endosome, MHC-I restricted epitopes can be rarely transported into ER for presentation [41]. It is suggested that the internalization of NCs can affect its presentation as well as signaling pathways for immunity [42]. Therefore, the minor difference in internalized pathway between Cs- and poly-amino-acid-based NCs may be the reason to cause such a subtle difference in DC proliferation here. Our findings also suggest the feasibility of positively charged NCs for DC therapy, which requires immune activators, such as LPS, to trigger DC uptake and activation [43]. Such activators induce DC activation along with several cytokines, increasing the risk of developing inflammatory and autoimmune diseases [44] and interfering with DC homeostasis [45]. The positively charged NC seems to activate and differentiate DCs without a cytokines storm like LPS. Combining its activity to induce Th1 response, the positively charged NC can be a potential immune activator ex vivo for DC therapy. Although the +NC contributing DC differentiation is clear here, receptors and downstream signaling pathways remain unknown. With further findings in mechanism, the precise control of +NC-induced immunity become possible.

5. Conclusion

In summary, using poly-anmino-acids to replace Cs and extra additives of saccharides, the immunomodulatory effect of +CNC were clarified. We found that a positive charge contributes to the immunological effect of NCs on Th responses by modulating DC differentiation. The positive charge plays a crucial role in differentiating DC populations to become CD8a^{+} cDC dominant. CD8a^{+} cDCs cross-present exogenous antigens to CD8^{+} T cells and are essential to generate cytotoxic effector T-cell responses [46]. In addition to activate CD4^{+} T cells, the +NCs activated CD8^{+} T cells in mice without safety concerns. Our finding addresses the mechanism of surface charge in activating Th1 response that for further developments of NC vaccines or even cell therapies.

Credit author statement

Yan-Wei Wu: Conceptualization, Methodology, Software, Validation, Formal analysis, Investigation, Writing - Original Draft, Visualization **Wan-Yu Wang:** Methodology, Software, Investigation, Data Curation, Formal analysis **Yu-Hung Chen (Corresponding author):** Conceptualization, Writing - Review & Editing, Supervision, Project administration, Funding acquisition.

Declaration of competing interest

The authors declare that they have no known competing financial interests or personal relationships that could have appeared to influence the work reported in this paper.

Data availability

Data will be made available on request.

Acknowledgements

We are grateful for the support for this study provided by BRIM Biotechnology, Taiwan, and Ascendo Biotechnology, Taiwan. The support for animals was provided by the Laboratory Animal Center, College of Medicine, National Cheng Kung University.

Appendix A. Supplementary data

Supplementary data to this article can be found online at https://doi.org/10.1016/j.mtbio.2022.100480.

References

[1] Y.K. Sung, S.W. Kim, Recent advances in polymeric drug delivery systems, Biomater. Res. 24 (1) (2020) 1–12, https://doi.org/10.1186/s40824-020-00190-7.
[2] C.K. Chen, P.K. Huang, W.C. Law, C.H. Chu, N.T. Chen, L.W. Lo, Biodegradable polymers for gene-delivery applications, Int. J. Nanomed. 15 (2020) 2131–2150, https://doi.org/10.2147/IJN.S222419.
[3] J. Panyam, V. Labhasetwar, Biodegradable nanoparticles for drug and gene delivery to cells and tissue, Adv. Drug Deliv. Rev. 55 (3) (2003) 329–347, https://doi.org/10.1016/s0169-409x(02)00228-4.
[4] K.G. Desai, Chitosan nanoparticles prepared by ionotropic gelation: an overview of recent advances, Crit. Rev. Ther. Drug Carrier Syst. 33 (2) (2016) 107–158, https://doi.org/10.1615/CritRevTherDrugCarrierSyst.2016014850.
[5] H.B.T. Moran, J.L. Turley, M. Andersson, E.C. Lavelle, Immunomodulatory properties of chitosan polymers, Biomaterials 184 (2018) 1–9, https://doi.org/10.1016/j.biomaterials.2018.08.054.
[6] Y.W. Wu, M.C. Chen, Y.H. Chen, Potential Zika vaccine: encapsulated nanocomplex promotes both TH1/TH2 responses in mice, Adv. Ther. 3 (3) (2020), 1900197, https://doi.org/10.1002/adtp.201900197.
[7] C.L. Bueter, C.K. Lee, V.A. Rathinam, G.J. Healy, C.H. Taron, C.A. Specht, S.M. Levitz, Chitosan but not chitin activates the inflammasome by a mechanism dependent upon phagocytosis, J. Biol. Chem. 286 (41) (2011) 35447–35455, https://doi.org/10.1074/jbc.M111.274936.
[8] C. Villiers, M. Chevallet, H. Diemer, R. Couderc, H. Freitas, A. Van Dorsselaer, P.N. Marche, T. Rabilloud, From secretome analysis to immunology: chitosan induces major alterations in the activation of dendritic cells *via* a TLR4-dependent mechanism, Mol. Cell. Proteomics 8 (6) (2009) 1252–1264, https://doi.org/10.1074/mcp.M800589-MCP200.
[9] S. Ravindranathan, B.P. Koppolu, S.G. Smith, D.A. Zaharoff, Effect of chitosan properties on immunoreactivity, Mar. Drugs 14 (5) (2016) 91, https://doi.org/10.3390/md14050091.
[10] S.E. McNeil, Nanotechnology for the biologist, J. Leukoc. Biol. 78 (3) (2005) 585–594.
[11] M.A. Dobrovolskaia, S.E. McNeil, Immunological properties of engineered nanomaterials, Nat. Nanotechnol. 2 (8) (2007) 469–478, https://doi.org/10.1038/nnano.2007.223.
[12] F. Sallusto, A. Lanzavecchia, The instructive role of dendritic cells on T-cell responses, Arthritis Res. 4 (Suppl 3) (2002) S127–S132, https://doi.org/10.1186/ar567.
[13] J. Saravia, N.M. Chapman, H. Chi, Helper T cell differentiation, Cell. Mol. Immunol. 16 (7) (2019) 634–643, https://doi.org/10.1038/s41423-019-0220-6.
[14] G. Sinani, M. Sessevmez, M.K. Gök, S. Özgümüş, H.O. Alpar, E. Cevher, Modified chitosan-based nanoadjuvants enhance immunogenicity of protein antigens after mucosal vaccination, Int. J. Pharm. 569 (2019), 118592, https://doi.org/10.1016/j.ijpharm.2019.118592.
[15] J. Khanifar, A.H. Salmanian, R. Haji Hosseini, J. Amani, R. Kazemi, Chitosan nanostructure loaded with recombinant E. coli O157:H7 antigens as a vaccine candidate can effectively increase immunization capacity, Artif. Cell Nanomed. Biotechnol. 47 (1) (2019) 2593–2604, https://doi.org/10.1080/21691401.2019.1629947.
[16] C. Korupalli, W.Y. Pan, C.Y. Yeh, P.M. Chen, F.L. Mi, H.W. Tsai, Y. Chang, H.J. Wei, H.W. Sung, Single-injecting, bioinspired nanocomposite hydrogel that can recruit host immune cells in situ to elicit potent and long-lasting humoral immune responses, Biomaterials 216 (2019), 119268, https://doi.org/10.1016/j.biomaterials.2019.119268.
[17] C.L. Bueter, C.A. Specht, S.M. Levitz, Innate sensing of chitin and chitosan, PLoS Pathog. 9 (1) (2013), e1003080, https://doi.org/10.1371/journal.ppat.1003080.
[18] A. Savina, S. Amigorena, Phagocytosis and antigen presentation in dendritic cells, Immunol. Rev. 219 (1) (2007) 143–156, https://doi.org/10.1111/j.1600-065X.2007.00552.x.
[19] A. Panariti, G. Miserocchi, I. Rivolta, Nanotechnol. The effect of nanoparticle uptake on cellular behavior: disrupting or enabling functions? Sci. Appl. 5 (2012) 87–100, https://doi.org/10.2147/NSA.S25515.
[20] K. Fytianos, L. Rodriguez-Lorenzo, M.J. Clift, F. Blank, D. Vanhecke, C. von Garnier, A. Petri-Fink, B. Rothen-Rutishauser, Uptake efficiency of surface modified gold nanoparticles does not correlate with functional changes and cytokine secretion in human dendritic cells in vitro, Nanomedicine 11 (3) (2015) 633–644, https://doi.org/10.1016/j.nano.2014.11.004.
[21] A.W. Purcell, J. McCluskey, J. Rossjohn, More than one reason to rethink the use of peptides in vaccine design, Nat. Rev. Drug Discov. 6 (5) (2007) 404–414, https://doi.org/10.1038/nrd2224.
[22] M. Merad, P. Sathe, J. Helft, J. Miller, A. Mortha, Annu. The dendritic cell lineage: ontogeny and function of dendritic cells and their subsets in the steady state and the inflamed setting, Rev. Immunol. 31 (2013) 563–604, https://doi.org/10.1146/annurev-immunol-020711-074950.
[23] J.H. Peters, R. Gieseler, B. Thiele, F. Steinbach, Dendritic cells: from ontogenetic orphans to myelomonocytic descendants, Immunol. Today 17 (6) (1996) 273–278, https://doi.org/10.1016/0167-5699(96)80544-5.
[24] D.A. Chistiakov, A.N. Orekhov, I.A. Sobenin, Y.V. Bobryshev, Plasmacytoid dendritic cells: development, functions, and role in atherosclerotic inflammation, Front. Physiol. 5 (2014) 279, https://doi.org/10.3389/fphys.2014.00279.
[25] D. Sichien, B.N. Lambrecht, M. Guilliams, C.L. Scott, Development of conventional dendritic Cells: from common bone marrow progenitors to multiple subsets in peripheral tissues, Mucosal Immunol. 10 (4) (2017) 831–844, https://doi.org/10.1038/mi.2017.8.
[26] R.M. Steinman, Z.A. Cohn, Identification of a novel cell type in peripheral lymphoid organs of mice. I. Morphology, quantitation, tissue distribution, J. Exp. Med. 137 (5) (1973) 1142–1162, https://doi.org/10.1084/jem.137.5.1142.
[27] Z. Shen, G. Reznikoff, G. Dranoff, K.L. Rock, Cloned dendritic cells can present exogenous antigens on both MHC class I and class II molecules, J. Immunol. 158 (6) (1997) 2723–2730.
[28] M.B. Lutz, R.M. Suri, M. Niimi, A.L. Ogilvie, N.A. Kukutsch, S. Rößner, G. Schuler, J.M. Austyn, Immature dendritic cells generated with low doses of GM-CSF in the absence of IL-4 are maturation resistant and prolong allograft survival in vivo, Eur. J. Immunol. 30 (7) (2000) 1813–1822, https://doi.org/10.1002/1521-4141(200007)30:7<1813::AID-IMMU1813>3.0.CO;2-8.
[29] L. van de Laar, P.J. Coffer, A.M. Woltman, Regulation of dendritic cell development by GM-CSF: molecular control and implications for immune homeostasis and therapy, Blood 119 (15) (2012) 3383–3393, https://doi.org/10.1182/blood-2011-11-370130.
[30] G.T. Belz, S.L. Nutt, Transcriptional programming of the dendritic cell network, Nat. Rev. Immunol. 12 (2) (2012) 101–113, https://doi.org/10.1038/nri3149.
[31] S.C. Eisenbarth, Dendritic cell subsets in T cell programming: location dictates function, Nat. Rev. Immunol. 19 (2) (2019) 89–103, https://doi.org/10.1038/s41577-018-0088-1.
[32] N. Oh, J.H. Park, Endocytosis and exocytosis of nanoparticles in mammalian cells, Int. J. Nanomed. 9 (Suppl 1) (2014) 51–63, https://doi.org/10.2147/IJN.S26592.
[33] C. David, M. Barrow, P. Murray, M.J. Rosseinsky, A. Owen, N.J. Liptrott, Vitro Determination of the immunogenic impact of nanomaterials on primary peripheral blood mononuclear cells, Int. J. Mol. Sci. 21 (16) (2020) 5610, https://doi.org/10.3390/ijms21165610.
[34] L.P. Jahromi, M.A. Shahbazi, A. Maleki, A. Azadi, H.A. Santos, Chemically engineered immune cell-derived microrobots and biomimetic nanoparticles: emerging biodiagnostic and therapeutic tools, Adv. Sci. 8 (8) (2021), 2002499, https://doi.org/10.1002/advs.202002499.
[35] F.S. Majedi, M.M. Hasani-Sadrabadi, Y. Kidani, T.J. Thauland, A. Moshaverinia, M.J. Butte, S.J. Bensinger, L.S. Bouchard, Cytokine secreting microparticles engineer the fate and the effector functions of T-cells, Adv. Mater. 30 (7) (2018), https://doi.org/10.1002/adma.201703178.
[36] C. Corbo, R. Molinaro, A. Parodi, N.E. Toledano Furman, F. Salvatore, E. Tasciotti, The impact of nanoparticle protein corona on cytotoxicity, immunotoxicity and target drug delivery, Nanomedicine 11 (1) (2016) 81–100, https://doi.org/10.2217/nnm.15.188.
[37] M. Cabeza-Cabrerizo, A. Cardoso, C.M. Minutti, M. Pereira da Costa, C. Reis e Sousa, Dendritic cells revisited, Annu. Rev. Immunol. 39 (2021) 131–166, https://doi.org/10.1146/annurev-immunol-061020-053707.
[38] K. Inaba, R.M. Steinman, M.W. Pack, H. Aya, M. Inaba, T. Sudo, S. Wolpe, G. Schuler, Identification of proliferating dendritic cell precursors in mouse blood, J. Exp. Med. 175 (5) (1992) 1157–1167, https://doi.org/10.1084/jem.175.5.1157.
[39] J. Helft, J. Bottcher, P. Chakravarty, S. Zelenay, J. Huotari, B.U. Schraml, D. Goubau, C. Reis e Sousa, GM-CSF mouse bone marrow cultures comprise a heterogeneous population of CD11c(+)MHCII(+) macrophages and dendritic cells,

Immunity 42 (6) (2015) 1197–1211, https://doi.org/10.1016/j.immuni.2015.05.018.
[40] R.J. Dress, C.A. Dutertre, A. Giladi, A. Schlitzer, I. Low, N.B. Shadan, A. Tay, J. Lum, M. Kairi, Y.Y. Hwang, E. Becht, Y. Cheng, M. Chevrier, A. Larbi, E.W. Newell, I. Amit, J. Chen, F. Ginhoux, Plasmacytoid dendritic cells develop from Ly6D(+) lymphoid progenitors distinct from the myeloid lineage, Nat. Immunol. 20 (7) (2019) 852–864, https://doi.org/10.1038/s41590-019-0420-3.
[41] M. Embgenbroich, S. Burgdorf, Current concepts of antigen cross-presentation, Front. Immunol. 9 (2018) 1643, https://doi.org/10.3389/fimmu.2018.01643.
[42] S. Patel, J. Kim, M. Herrera, A. Mukherjee, A.V. Kabanov, G. Sahay, Brief update on endocytosis of nanomedicines, Adv. Drug Deliv. Rev. 144 (2019) 90–111, https://doi.org/10.1016/j.addr.2019.08.004.
[43] L. Castiello, M. Sabatino, P. Jin, C. Clayberger, F.M. Marincola, A.M. Krensky, D.F. Stroncek, Monocyte-derived DC maturation strategies and related pathways: a transcriptional view, Cancer Immunol. Immunother. 60 (4) (2011) 457–466, https://doi.org/10.1007/s00262-010-0954-6.
[44] P. Blanco, A.K. Palucka, V. Pascual, J. Banchereau, Dendritic cells and cytokines in human inflammatory and autoimmune diseases, Cytokine Growth Factor Rev. 19 (1) (2008) 41–52, https://doi.org/10.1016/j.cytogfr.2007.10.004.
[45] M. Merad, M.G. Manz, Dendritic cell homeostasis, Blood 113 (15) (2009) 3418–3427, https://doi.org/10.1182/blood-2008-12-180646.
[46] K. Shortman, W.R. Heath, The CD8+ dendritic cell subset, Immunol. Rev. 234 (1) (2010) 18–31, https://doi.org/10.1111/j.0105-2896.2009.00870.x.